

Structural Changes in Bacteriorhodopsin Caused by Two-Photon-Induced Photobleaching

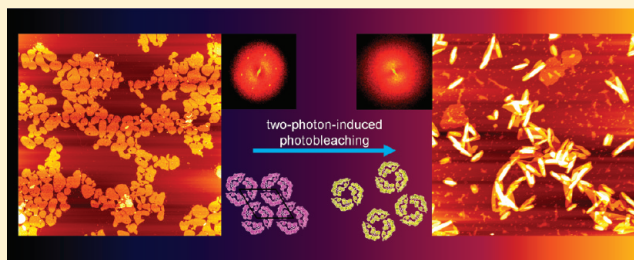
Daniel Rhinow,[†] Martin Imhof,[‡] Ivan Chizhik,[‡] Roelf-Peter Baumann,[‡] and Norbert Hampp*,^{*,‡,§}

[†]Department of Structural Biology, Max-Planck-Institute of Biophysics, Max-von-Laue-Str. 3, D-60438 Frankfurt, Germany

[‡]Department of Chemistry, Philipps-University of Marburg, Hans-Meerwein-Str. Bldg. H, D-35032 Marburg, Germany

[§]Material Sciences Center, D-35032 Marburg, Germany

ABSTRACT: Bacteriorhodopsin (BR) is the key protein of the halobacterial photosynthetic system. BR assembles into two-dimensional crystalline patches, the so-called purple membranes (PM), and acts as a light-driven proton pump converting light energy into the chemical energy of a proton gradient over the cell membrane. The two-photon absorption (TPA) of BR is so far not fully understood. Astonishingly high TPA cross sections have been reported, but the molecular mechanisms have not been elucidated. In this work, we address structural changes in BR and PM upon TPA, investigating its TPA photochemistry by spectroscopy, small-angle X-ray scattering, as well as electron and atomic force microscopy. We observe that TPA of BR leads to formation of an UV-absorbing *N*-retinyl-bacterioopsin state, which is accompanied by the loss of crystalline order in PM. FTIR and CD spectroscopy confirm that BR trimers as well as the secondary structure of the BR molecules are preserved. We demonstrate that excitation by TPA results in the photochemical reduction of the retinal Schiff base, which in turn causes a permanent asymmetric shape change of BR, similar to the one transiently observed during the photocycle-related opening and closing of the cytoplasmic proton half channel. This shape change causes PM sheets to merely roll up toward the extracellular side and causes the loss of crystallinity of PM. We present a model for the TPA photoresponse of BR, which also explains the irreversibility of the process in terms of a photochemical reduction of the Schiff base.



INTRODUCTION

Bacteriorhodopsin (BR) is a light-driven proton pump, which is found in the so-called purple membrane (PM) of *Halobacterium salinarum*.^{1–4} PM sheets are two-dimensional crystals, which consist of BR and lipids only.^{1,4} BR is the paradigm of seven transmembrane helix proteins and shares profound homology with other retinal proteins.^{5–12} High-resolution structural analysis of BR and PM has revealed a detailed molecular picture of light-dependent proton transport across the cell membrane.^{13–18} Upon absorption of a photon of visible light, BR undergoes a cyclic series of photochemical transitions (Figure 1a), which are spectroscopically distinguishable by their optical absorption maxima.² Because of its photochromic properties, along with its astonishing chemical robustness and thermal stability, BR shows great promise for technical applications such as data storage or optical devices.^{19–21} Most spectroscopic investigations refer to low light intensities where a single photon is absorbed by BR. Besides an extraordinarily high molar extinction coefficient, due to spectral tuning of retinal by specific amino acid residues in the binding pocket,²² BR has an extremely high cross section for two-photon absorption.²³ In earlier work, it has been demonstrated that two-photon excitation of BR leads to the formation of distinct photoproducts beyond the classical photocycle.^{24–26}

The interest in studying two-photon-induced processes in BR is twofold. First, from a fundamental point of view, molecular properties not accessible to classical single-photon

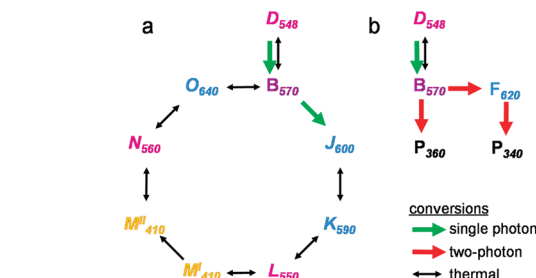


Figure 1. Photoreactions of BR. (a) The BR photocycle. Single-photon absorption is indicated by green arrows. (b) Two-photon excitation of BR (indicated by red arrows) leads to formation of a blue-shifted intermediate (F_{620}) along with photochemical species absorbing in the UV range. The experiments suggest that BR_{340}^{TPP} is formed upon photobleaching of the F_{620} intermediate, whereas BR_{360}^{TPP} is a direct photoproduct of BR_{570} .

excitation can be analyzed.²⁷ Second, due to the quadratic dependence on the field intensity, two-photon-induced processes can be triggered with extremely high spatial resolution,^{28,29} which makes them attractive for data storage using two-photon-excitable materials.^{23,25,30–32} Upon irradiation of PM with

Received: November 23, 2011

Revised: April 10, 2012

Published: April 18, 2012

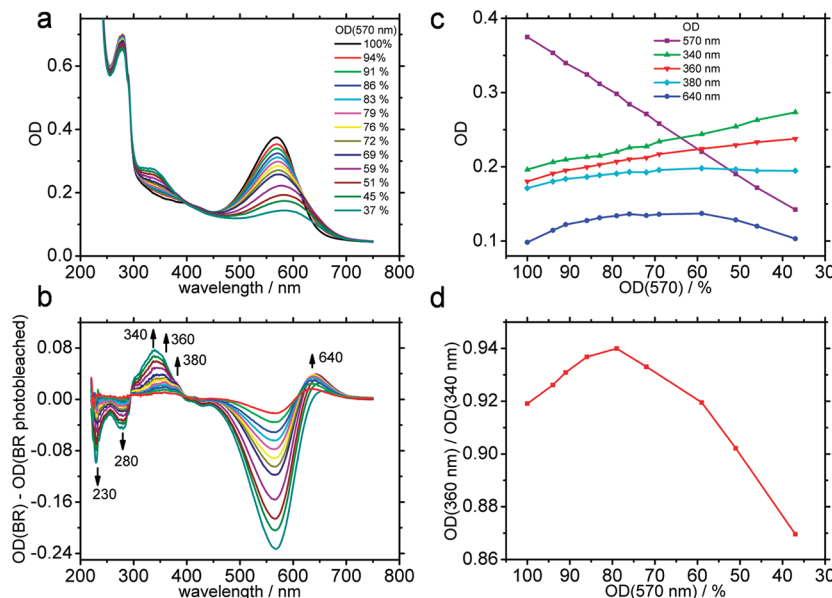


Figure 2. Spectral changes in the UV–vis region of the optical spectrum upon two-photon-induced photobleaching of BR. (a) Dose dependent UV–vis spectra. As a measure for the progress in photobleaching, we chose the OD of photobleached BR at 570 nm compared to its initial value. (b) Difference spectra. The colors correspond to those in part a. Upon photobleaching, a blue-shifted photoproduct, previously named the F-state,²⁴ is formed along with a photoproduct with absorption bands around 360 nm. Intensity losses at 280 and 230 nm are visible, which are most likely due to decreasing interactions between retinal and aromatic amino acids, especially tryptophan and tyrosine. (c) Dose-dependent ODs at selected wavelengths. (d) Plot of the ratio OD(360 nm)/OD(340 nm). The amount of BR^{TPP}₃₄₀ formed correlates with photobleaching of the red-shifted photoproduct.

intense laser pulses, BR₅₇₀ is converted to the red-shifted F₆₂₀-state,²⁵ which is subsequently photoconverted to yield distinguishable photoproducts with absorption maxima around 360 nm (Figure 1b). The kinetics of the participating two-photon reactions have been studied in detail,^{25,26} and the possibility of data storage using two-photon-induced anisotropy in BR films has been demonstrated.^{25,33,34} However, the structural changes in BR and PM accompanying two-photon-induced photobleaching have not yet been investigated. Information about two-photon-induced structural changes in BR and PM improve our mechanistic understanding of two-photon data storage in BR.

In this work, we combine structural studies by small-angle X-ray scattering (SAXS), transmission electron microscopy (TEM), and atomic force microscopy (AFM) with Fourier transform infrared (FT-IR) spectroscopy and circular dichroism (CD) to analyze structural changes in BR upon two-photon-induced photobleaching (TPP). We demonstrate that TPP of BR leads to a loss of crystallinity of PM but causes only minor changes in the bacteriorhodopsin scaffold. We show that TPP of BR is accompanied by considerable bending and curling of the corresponding membranes. We discuss the mechanisms of TPP of BR and give a comparative analysis with other modes of BR photobleaching, described in the earlier literature.^{35–38}

■ EXPERIMENTAL METHODS

Materials. PM was freshly purified according to standard procedures.³⁹

Two-Photon-Induced Photobleaching of BR in Suspension. Wildtype PM was suspended in distilled water, transferred to quartz cuvettes, and irradiated with a frequency doubled Nd:YAG laser (Infinity 40-100, Coherent Inc.) operating at 532 nm (pulse length 3 ns, repetition rate 20 Hz).

Small Angle X-ray Scattering (SAXS). Oriented PM multilayers were prepared from PM suspended in distilled water as described previously.⁴⁰ PM suspensions were deposited on a thin plastic substrate and slowly air-dried overnight. PM multilayers were analyzed with a SAXS camera comprising a Phillips PW1830 X-ray generator and a KKK-type Kratky camera (Anton Paar, Graz, Austria) with a sample–detector distance of 200 mm.

Transmission Electron Microscopy (TEM). PM suspensions were placed between two small copper disks and plunged into liquid ethane. Replicas were prepared in a Balzers BAF 400T freeze-fracture unit at 3×10^{-7} mbar keeping the specimen stage at -130°C . Shadowing with Pt/C was performed at an angle of 45° , followed by evaporation of pure carbon at 90° to reinforce the heavy metal replica. Replicas were thawed, cleaned from organic material in chromosulfuric acid, and imaged with an EM208S electron microscope (FEI, Hillsboro, USA).

Fourier Transform Infrared (FTIR) Spectroscopy. FT-IR spectra were recorded on a Perkin-Elmer FT-IR spectrometer (1600 series), at a resolution of 2 cm^{-1} . Background-corrected spectra were deconvoluted ($k = 1.6$) using the program Win-IR Pro (DigiLab).

Atomic Force Microscopy (AFM). **AFM of PM Sheets Laser-Irradiated in Situ.** A $20\text{ }\mu\text{L}$ portion of PM suspension ($\text{OD}(\text{BR}_{570}^{\text{initial}}) = 0.3$) was incubated on freshly cleaved mica for 10 min. Samples were washed with deionized water and dried in air prior to laser irradiation. PMs were irradiated in situ with a QuikLaze 50ST2/Trilite (New Wave Research) operating at 532 nm with a repetition rate of 50 Hz and a pulse length of 4 ns. The diameter of the focused spot was $1\text{ }\mu\text{m}$. Laser-irradiated PMs along these lines were analyzed by AFM in tapping mode in air with a Nanoscope IV with multimode controller (Bruker).

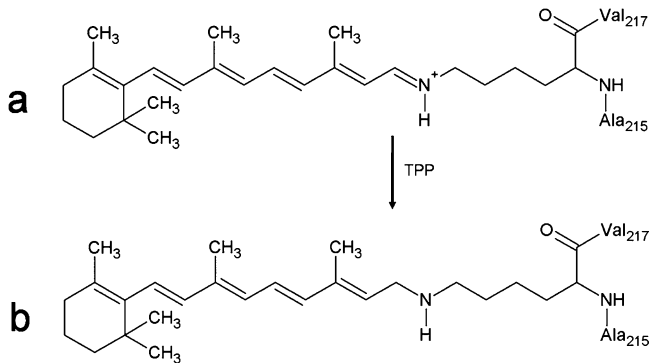


Figure 3. Reduction of the retinal Schiff base upon two-photon-induced photobleaching of BR. (a) Structure of retinal bound to lysine-216 in the binding pocket of BR. (b) Structure of the *N*-retinyl species formed upon two-photon-induced photobleaching of BR.

Tapping Mode AFM in Air. An $\sim 10 \mu\text{L}$ portion of photobleached PM suspension ($\text{OD}(\text{BR}_{570}^{\text{initial}}) = 0.3$) was pipetted onto freshly cleaved mica, dried in air, and subsequently analyzed by tapping mode AFM using a Nanoscope IV with multimode controller (Bruker).

Contact Mode AFM in Liquid. A $5 \mu\text{L}$ portion of photobleached PM suspension ($\text{OD}(\text{BR}_{570}^{\text{initial}}) = 0.3$) was pipetted together with $50 \mu\text{L}$ of imaging buffer (300 mM KCl, pH 3.4) onto freshly cleaved mica. After 20 min of incubation, excess material was removed by extensive rinsing with imaging buffer. The samples were then mounted on the sample stage and were allowed to reach thermal equilibrium (30 min) before analysis. AFM imaging was performed in liquid (imaging buffer) in a Nanoscope IV system with multimode controller (Bruker).

Force Spectroscopy. Single molecule force spectroscopy was used to differentiate between the cytoplasmatic and extracellular side of PM. Peak positions and interpeak distances were determined according to the worm-like chain model.

RESULTS AND DISCUSSION

Spectral Changes in the UV-vis Region of the Optical Spectrum

Spectral Changes in the UV-vis Region of the Optical Spectrum. Irradiation of BR suspensions with intense 532 nm laser pulses leads to the formation of distinct photoproducts which were analyzed by UV-vis spectroscopy (Figure 2). Dose-dependent UV-vis difference spectra (Figure 2b) reveal that in the course of two-photon-induced photobleaching BR_{570} is converted to both a red-shifted photoproduct (F-state)²⁵ and a blue-shifted photoproduct with absorption bands around 360 nm ($\text{BR}_{340}^{\text{TPP}}$, $\text{BR}_{360}^{\text{TPP}}$, and $\text{BR}_{380}^{\text{TPP}}$), consistent with earlier observations.^{24–26} Figure 2c shows the changes in optical density (OD) at selected wavelengths as a function of the degree of photobleaching. As a measure of photobleaching, we chose the OD of photobleached BR_{570} compared to its initial OD, $\text{OD}(\text{BR}_{570}^{\text{initial}})$. During TPP of BR, the initial state, BR_{570} , is increasingly consumed. Likewise, the red-shifted F-state, which is formed initially, is photoconverted upon further photobleaching. Over the course of the experiment, a photoproduct with peaks at 340, 360, and 380 nm is formed continuously, resembling the end product of TPP of BR. The formation of the photoproduct is accompanied by a loss of absorption at 280 and 230 nm. Because similar observations have been made on chemical reduction of the Schiff base,³⁵ we conclude that the loss of absorption at 280 and 230 nm is due to weaker interactions between retinal and tryptophan and tyrosine residues in the binding pocket. We observed a correlation

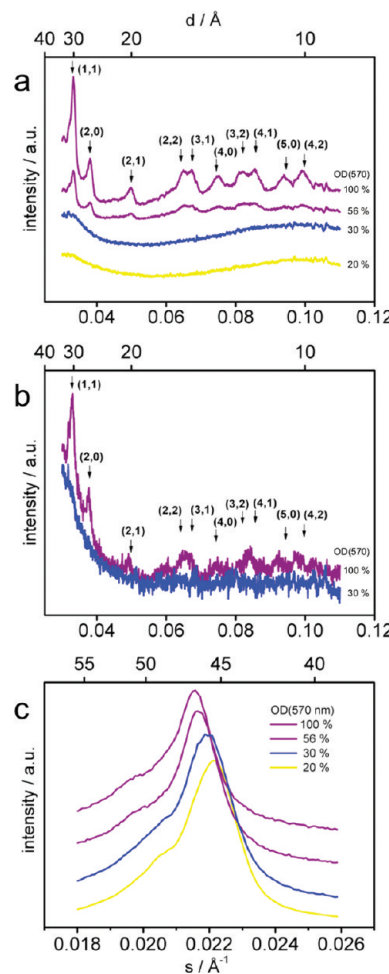


Figure 4. Small-angle X-ray scattering (SAXS) of photobleached PM sheets. (a) Scattering profiles of dried PM multilayers obtained from increasingly photobleached PM. The 100% value refers to the initial absorption at 570 nm. Percent values give the absorption at 570 nm retained. Upon increasing photobleaching, the crystallinity of PM is lost. (b) Scattering profiles obtained from photobleached PM in suspension. (c) Scattering profiles of PM multilayers recorded with the X-ray beam incident in a direction parallel to the membrane multilayer. The maxima indicate the lamellar thickness of PM. In the course of two-photon photobleaching, the average thickness of PM decreases from 46.5 to 45.5 Å.

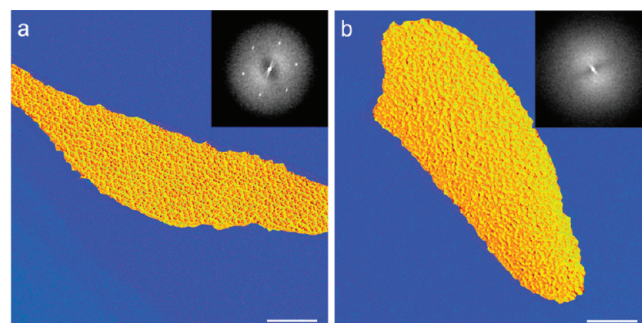


Figure 5. Freeze-fracture transmission electron microscopy of photobleached PM. (a) Native PM. (b) PM after two-photon photobleaching to $\sim 30\%$ of initial optical density $\text{OD}(\text{BR}_{570}^{\text{initial}})$. The crystalline lattice is completely lost. The insets show Fourier transforms of the images. Scale bars are 100 nm.

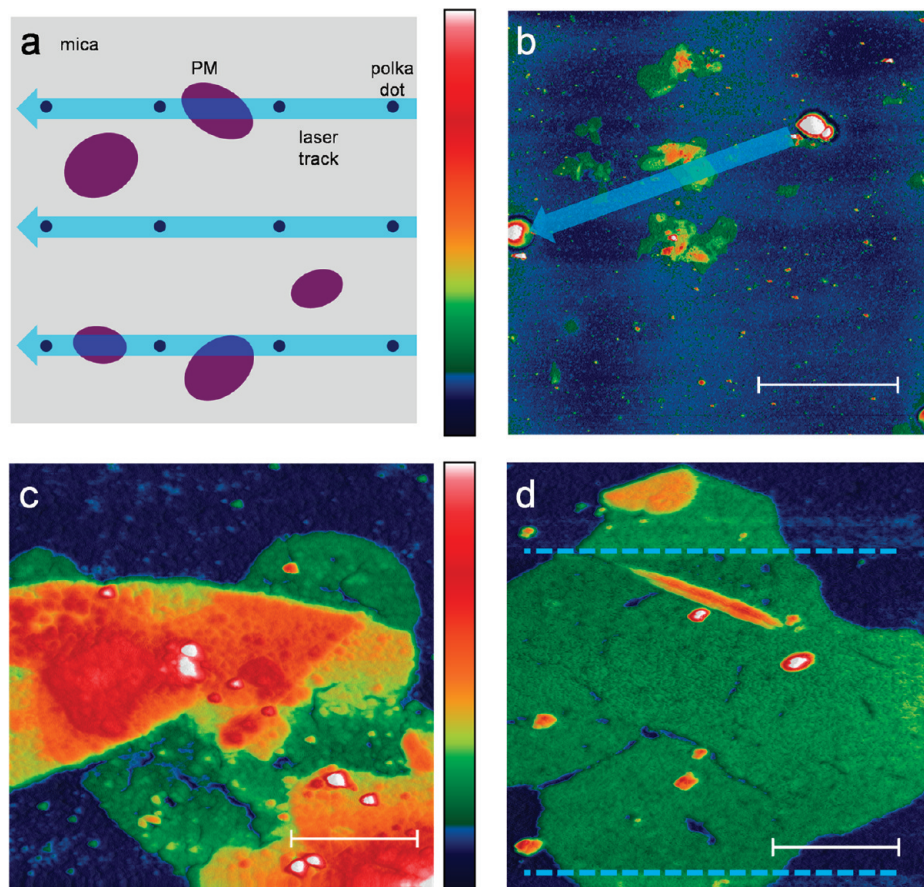


Figure 6. Atomic force microscopy (AFM) of laser-irradiated PM. (a) Outline of the experiment. PM sheets are prepared on mica in buffer, washed with water, air-dried, laser-irradiated, and subsequently analyzed by AFM in air. (b) Laser-irradiated PM. The track of the laser beam is indicated (arrow). Two dots are visible, which are laser marks in the substrate to identify laser-irradiated PM in the AFM. The dots are at either end of the arrow. The height scale is 50 nm. The scale bar is 5 μ m. (c) Close-up view of the laser-irradiated PM shown in part b. The AFM images reveal cracks and distortions in the PM in response to the intense laser beam. The height scale is 25 nm. The scale bar is 500 nm. (d) A large single PM sheet laser-irradiated in the center (area indicated by dashed lines). Cracks and distortions indicate the impact of the laser beam. The height scale is 25 nm. The scale bar is 500 nm.

between the formation of $\text{BR}_{340}^{\text{TPP}}$ and photobleaching of the F-state. Figure 2d shows the ratio of $\text{OD}_{360 \text{ nm}}/\text{OD}_{340 \text{ nm}}$. Initially, $\text{BR}_{360}^{\text{TPP}}$ is the main species, formed along with the F-state upon photobleaching of BR. As soon as the F-state is photoconverted, increasingly more $\text{BR}_{340}^{\text{TPP}}$ is formed, thus decreasing the $\text{OD}(360 \text{ nm})/\text{OD}(340 \text{ nm})$ ratio. The observations suggest that $\text{BR}_{360}^{\text{TPP}}$ is the main species of TPP of BR_{570} , whereas formation of $\text{BR}_{340}^{\text{TPP}}$ is mainly due to subsequent photobleaching of the F-state (Figure 1b). With exception of the red-shifted F-state, the species formed upon TPP of BR are identical to the main species formed upon BR reduction by NaBH_4 , that are $\text{BR}_{340}^{\text{red}}$, $\text{BR}_{360}^{\text{red}}$, and $\text{BR}_{380}^{\text{red}}$.³⁵ It is worth noting that an analogous photoproduct has been observed upon treatment of PM suspensions with short electron pulses.³⁶ The chemical mechanisms of radiation-induced reduction of BR have been analyzed and revealed hydrogen radicals as main species responsible for Schiff base reduction and N-retinyl-bacteriorhodopsin as the photoproduct.^{36,41} N-Retinyl-bacteriorhodopsin is characterized by a three-peaked absorption band. BR_{340} , BR_{360} , and BR_{380} resemble different rotamers of the retinyl chromophore. Therefore, it is reasonable to assume that TPP of BR involves reduction of the Schiff base by hydrogen radicals generated upon two-photon absorption by retinal and subsequent formation of N-retinyl-bacteriorhodopsin (Figure 3).

Structural Changes in the Crystalline Assembly of PM.

Changes in the crystalline assembly of PM were analyzed by small-angle X-ray scattering (SAXS) of oriented PM multilayers obtained from photobleached PM in suspension. Figure 4a demonstrates that TPP of BR is accompanied by a progressive loss of the two-dimensional crystalline assembly of PM. As soon as $\text{OD}(\text{BR}_{570})$ falls below $\sim 30\%$ of its initial value, diffraction is no longer observed. To exclude drying artifacts, which in the past have hampered structure determination of cation-free PM,⁴² we recorded SAXS data from suspended PMs (Figure 4b). In contrast to native PM, which showed regular Bragg diffraction maxima, no diffraction was observed with suspended PM photobleached to 30% $\text{OD}(\text{BR}_{570}^{\text{initial}})$, similar to dried PM films. In the course of TPP of BR, the measured thickness of PM decreases from 46.5 Å (100% $\text{OD}(\text{BR}_{570}^{\text{initial}})$) to 45.5 Å (20% $\text{OD}(\text{BR}_{570}^{\text{initial}})$), as demonstrated by SAXS of oriented PM multilayers analyzed incident in a direction parallel to the membrane multilayer (Figure 4c).

In addition to SAXS analysis, which gives statistical information about ensembles, we also analyzed structural changes in PM on the level of single membranes. Figure 5 shows images of PM obtained by freeze-fracture transmission electron microscopy of PM suspensions. The two-dimensional crystalline lattice of PM is visible before TPP (Figure 5a). In samples photobleached

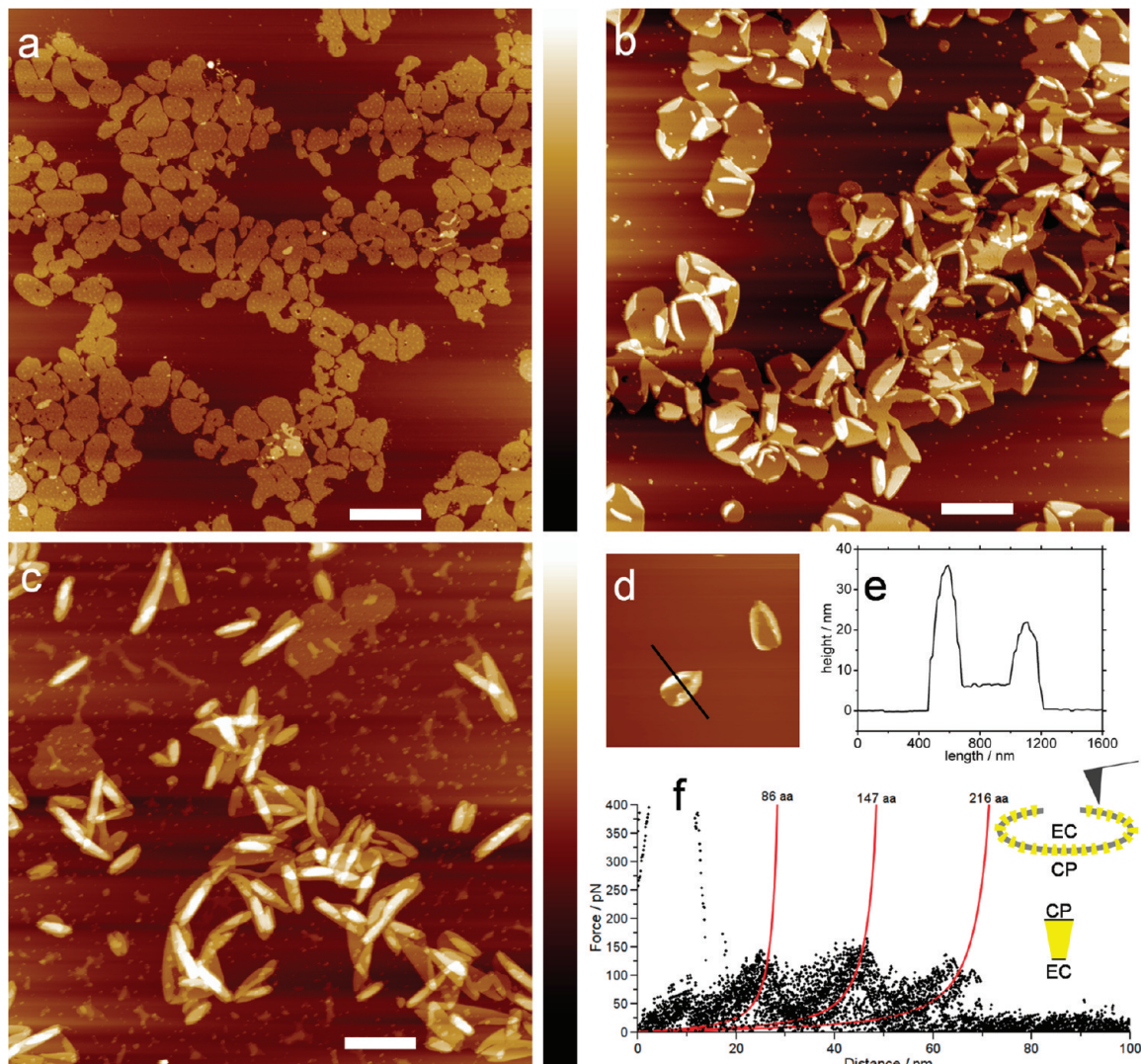


Figure 7. Bending and curling of PM sheets upon two-photon-induced photobleaching. (a) Native PM. AFM image of dried PM sheets on mica. (b) AFM image of PM photobleached to $\sim 30\%$ OD($BR_{570}^{initial}$). (c) AFM image of PM photobleached to $\sim 10\%$ OD($BR_{570}^{initial}$). (d) AFM image of PM in liquid, photobleached to $\sim 20\%$ OD($BR_{570}^{initial}$). (e) Line section across a single PM. (f) Cytoplasmatic force spectra recorded from the curled rim (as sketched in the small inset) of bent PM sheets reveal that PM sheets curl toward the extracellular side upon TPP.

to levels below 30% OD($BR_{570}^{initial}$), the lattice is no longer observed (Figure 5b). TEM analysis thus confirms the results obtained by SAXS on the level of single membranes.

To analyze the impact of laser irradiation on immobilized single PM sheets, we performed tapping-mode atomic force microscopy (TM-AFM) on laser-irradiated membranes *in situ*. For the laser-irradiation procedure, first a regular dot grid pattern (polka dots) was laser-marked on the mica substrate with the 532 nm laser of the QuikLaze Trilite system. The resulting regular grid of “points” is easily recognized in the finder microscope on top of the AFM. Then, the connecting lines between the dots were laser-irradiated using single pulses of lower laser intensity (see Figure 6a). Laser-irradiated PMs, located on the connecting lines between two dots, were identified and analyzed by TM-AFM. Figure 6b shows an overview AFM image of a laser-irradiated PM. The track of the laser beam is indicated by an arrow. A close-up view of the same laser-irradiated PM is shown in Figure 6c. We could not detect the crystalline lattice. Cracks are visible, which were formed in response to the laser beam. Figure 6c supports this, as the membrane shown has only been irradiated in the central

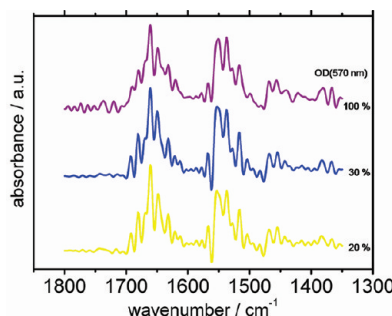


Figure 8. Fourier transform infrared (FT-IR) spectroscopy of photobleached PM. The amide-I peak at 1661 cm^{-1} , indicative of a regular trimeric assembly of BR, is virtually unchanged upon two-photon-induced photobleaching. The spectra indicate no changes in BR secondary structure, even after heavy photobleaching to $\sim 20\%$ OD($BR_{570}^{initial}$), indicating that the bacteriorhodopsin structure as well as the trimer remain intact.

region where cracks and fissures can be identified. However, the crystalline lattice could not be resolved in either case.

Two-Photon-Induced Changes in PM Topology. An AFM image of native PM is shown in Figure 7a. Upon TPP, the topology of PM changes considerably. Parts b and c of Figure 7 show AFM images of PM photobleached to $\sim 30\%$ OD($BR_{570}^{initial}$) and $\sim 10\%$ OD($BR_{570}^{initial}$), respectively. Images were recorded by TM-AFM of PM dried on mica. The images demonstrate that

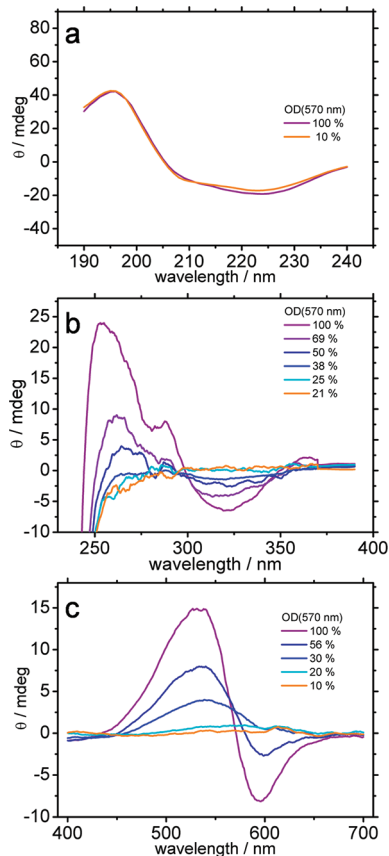


Figure 9. Circular dichroism (CD) of photobleached BR. (a) CD in the UV region. The spectra reveal only minor changes in BR secondary structure even after photobleaching to $\sim 10\%$ OD($BR_{570}^{initial}$). (b) CD in the UV/near-UV region. In the course of two-photon-induced photobleaching, the CD activity of tryptophans (~ 260 nm) disappears. The CD signal at ~ 315 nm has been attributed to an electrically forbidden but magnetically allowed dipole transition.⁴⁷ (c) CD in the visible region. The CD spectrum of native BR reveals the well-known biphasic band of the retinal chromophore. Upon photobleaching, the biphasic spectrum is converted to a monophasic spectrum, indicative of conformational relaxation in the retinal binding pocket. Finally, the CD signal at ~ 540 nm is lost.

TPP of BR is accompanied by progressive bending and curling of the membrane. To exclude drying artifacts, we analyzed the topology of photobleached PM by contact mode AFM in liquid. Figure 7d shows an AFM image of PM photobleached to $\sim 30\%$ OD($BR_{570}^{initial}$). The image was recorded by contact mode AFM in liquid. A line section across a bent PM is presented in Figure 7e. Force spectroscopy revealed that PM, containing mainly BR_{340}^{TPP} , BR_{360}^{TPP} , and BR_{380}^{TPP} , bends toward the extracellular side (Figure 7f). Small distortions of Schiff base counterion interactions are sufficient to produce large scale conformational changes in BR.⁴³ In earlier publications, we demonstrated that collective conformational changes result in strong bending of PM due to the wedge-shaped M-state-like BR molecules.^{44,45} The strong bending of PM sheets as revealed by AFM analysis, suggests that loss of the positive charge on the Schiff base upon TPP leads to opening of the cytoplasmatic half channel as well. To minimize the surface tension, caused by the asymmetric shape of the BRs, a shape change of the PM sheets occurs and they roll up, starting from the outer rim.

BR Secondary Structure, Trimer Assembly, and Retinal Binding Pocket. Although analysis by SAXS, TEM, and AFM revealed substantial structural changes at the level of PM assembly, Fourier transform infrared (FTIR) spectroscopy and circular dichroism (CD) indicate only minor changes in BR secondary structure and trimer assembly upon TPP. Figure 8 shows FTIR spectra of PM films obtained from photobleached PM suspension. All samples show the amide-I band centered around 1661 cm^{-1} indicative of individual BRs arranged in regular trimers.⁴⁶ Interestingly, similar observations have been made with PM photobleached with hydroxylamine.^{37,38} In the course of photobleaching with hydroxylamine, the crystalline assembly of PM is disrupted,^{37,38} thus resembling our results on TPP of BR. Likewise, the BR trimer is unchanged.³⁸ Upon TPP, no loss of secondary structure is observed. Similar results were obtained by CD analysis of BR photobleached in suspension. Figure 9a shows CD spectra of photobleached BR in the UV region, which contain information about the secondary structure of the bacteriorhodopsin scaffold. Even after photobleaching to 10% OD($BR_{570}^{initial}$), no significant changes in secondary structure were observed. Figure 9b shows CD spectra of photobleached BR in the UV/near-UV region. Noteworthy, photoproducts BR_{340}^{TPP} , BR_{360}^{TPP} , and BR_{380}^{TPP} are not CD-active. This is in contrast to BR_{340}^{red} , BR_{360}^{red} , and BR_{380}^{red} , the products of chemical reduction of the BR Schiff base, which produce a strong CD signal around 360 nm .⁴⁷ The missing CD activity indicates a relaxation of conformational constraints in the retinal binding pocket. Increasing conformational freedom of tryptophan residues is probably responsible for decreasing

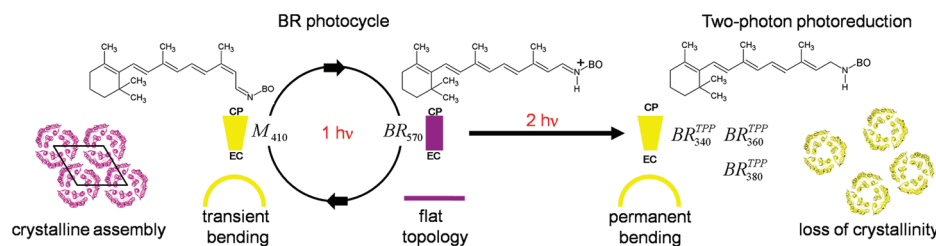


Figure 10. Structural changes in BR and PM upon two-photon-induced photobleaching compared to the classical photocycle. Two-photon-induced photobleaching of BR generates N-retinyl-bacteriorhodopsin species, which are characterized by a neutral Schiff base, analogous to M-state BR in the classical photocycle. Wedge-shaped BRs and bent PM sheets are transiently formed in the classical photocycle, whereas two-photon-induced photobleaching of BR causes an irreversible structural change, leading to permanently wedge-shaped BRs. As a consequence, PM sheets merely roll up and the crystallinity is lost.

CD activity at ~ 260 nm. The CD signal at ~ 315 nm has been attributed to an electrically forbidden but magnetically allowed dipole transition.⁴⁷ Before photobleaching, BR₅₇₀ gives rise to a biphasic signal in the visible CD spectrum (Figure 9c), consistent with earlier observations.⁴⁷ Upon TPP, the biphasic CD band is converted into a monophasic band, as also observed in chemical reduction of BR⁴⁷ as well as in photobleaching of reconstituted BR.⁴⁸ This is a further indication of released constraints in the binding pocket.

CONCLUSIONS

We have demonstrated that TPP of BR has a major impact on the crystallinity and topology of PM, which is caused by minor structural changes at the level of individual BR molecules. Figure 10 summarizes the structural changes in BR and PM upon TPP in comparison to the classical BR photocycle. Two-photon excitation of the retinal chromophore leads to generation of hydrogen radicals, reducing the Schiff base. In the course of the process, well-defined UV-absorbing states are generated. UV-vis spectroscopy revealed that BR₃₄₀^{TPP} is formed by photobleaching of F₆₂₀, a red-shifted intermediate,²⁵ whereas BR₃₆₀^{TPP} is formed upon direct photoexcitation of BR₅₇₀. As shown by FTIR spectroscopy, the formation of N-retinylbacteriopsin leaves the trimeric assembly of BR unchanged. Furthermore, FTIR and CD spectroscopy confirmed that the secondary structure of bacteriorhodopsin is preserved. However, irreversible loss of the positive charge at the Schiff base upon phototriggered reduction leads to formation of wedge-shaped BR, analogous to the M-state of BR. Accumulation of wedge-shaped BRs leads to strong bending of PM, shown by AFM, and causes weakening of the crystalline assembly (SAXS, TEM, AFM). The phototriggered Schiff base reduction causes shape changes on the molecular level of BR, and in turn results in loss of PM crystallinity. This explains the irreversible molecular and functional changes occurring during two-photon-absorption-induced photobleaching of bacteriorhodopsin.

AUTHOR INFORMATION

Corresponding Author

*Phone: +49 6421 2825775. Fax: +49 6421 2825798. E-mail: hampp@staff.uni-marburg.de.

Notes

The authors declare no competing financial interest.

ACKNOWLEDGMENTS

We thank Friederike Joos (MPI of Biophysics, Frankfurt) for freeze-fracture electron microscopy. PM was a gift from Dieter Oesterhelt's lab at the Max Planck Institute of Biochemistry, Martinsried, Germany. We thank Werner Kühlbrandt (MPI of Biophysics, Frankfurt) for a critical reading of the manuscript.

REFERENCES

- Oesterhelt, D.; Stoeckenius, W. *Nat. New Biol.* **1971**, *233*, 149–152.
- Haupts, U.; Tittor, J.; Oesterhelt, D. *Annu. Rev. Biophys. Biomol. Struct.* **1999**, *28*, 367–399.
- Lanyi, J. K. Bacteriorhodopsin. *Annu. Rev. Physiol.* **2004**, *66*, 665–688.
- Krebs, M. P.; Isenbarger, T. A. *Biochim. Biophys. Acta* **2000**, *1460*, 15–26.
- Kolbe, M.; Hüseyin, B.; Essen, L.-O.; Oesterhelt, D. *Science* **2000**, *288*, 1390–1396.
- Luecke, H.; Schobert, B.; Lanyi, J. K.; Spudich, E. N.; Spudich, J. L. *Science* **2001**, *293*, 1499–1503.
- Royant, A.; Nollert, P.; Edman, K.; Neutze, R.; Landau, E. M.; Pebay-Peyroula, E.; Navarro, J. *Proc. Natl. Acad. Sci. U.S.A.* **2001**, *98*, 10131–10136.
- Gordeliy, V. I.; Labahn, J.; Moukhametzianov, R.; Efremov, R.; Granzin, J.; Schlesinger, B.; Büldt, G.; Savopol, T.; Scheidig, A. J.; Klare, J. P.; et al. *Nature* **2002**, *419*, 484–487.
- Vogley, L.; Sineshevskov, O. A.; Vishwa, D. T.; Sasaki, Jun.; Spudich, J.; Luecke, H. *Science* **2004**, *306*, 1390–1393.
- Balashov, S. P.; Imasheva, E. S.; Boichenko, V. A.; Antón, J.; Wang, J. M.; Lanyi, J. K. *Science* **2005**, *309*, 2061–2064.
- Spudich, J. L. *Trends Microbiol.* **2006**, *14*, 480–487.
- Friedrich, T.; Geibel, S.; Kalmbach, R.; Chizhov, I.; Ataka, K.; Heberle, J.; Engelhard, M.; Bamberg, E. *J. Mol. Biol.* **2002**, *321*, 821–838.
- Grigorieff, N.; Ceska, T. A.; Downing, K. H.; Baldwin, J. M.; Henderson, R. *J. Mol. Biol.* **1996**, *259*, 393–421.
- Kimura, Y.; Vassylyev, D. G.; Miyazawa, A.; Kidera, A.; Matsushima, M.; Mitsuoka, K.; Murata, K.; Hirai, T.; Fujiyoshi, Y. *Nature* **1997**, *389*, 206–211.
- Essen, L.-O.; Siegert, R.; Lehmann, W. D.; Oesterhelt, D. *Proc. Natl. Acad. Sci. U.S.A.* **1998**, *95*, 11673–11678.
- Luecke, H.; Schobert, B.; Richter, H.-T.; Cartailler, J.-P.; Lanyi, J. *J. Mol. Biol.* **1999**, *291*, 899–911.
- Sass, H. J.; Büldt, G.; Gessenich, R.; Hehn, D.; Neff, D.; Schlesinger, R.; Berendzen, J.; Ormos, P. *Nature* **2000**, *406*, 649–653.
- Subramaniam, S.; Henderson, R. *Nature* **2000**, *406*, 653–657.
- Oesterhelt, D.; Bräuchle, C.; Hampp, N. *Q. Rev. Biophys.* **1991**, *24*, 425–478.
- Birge, R. R. *Annu. Rev. Phys. Chem.* **1990**, *41*, 683–733.
- Hampp, N. *Chem. Rev.* **2000**, *100*, 1755–1778.
- Hayashi, S.; Tajkhorshid, E.; Pebay-Peyroula, E.; Royant, A.; Landau, E. M.; Navarro, J.; Schulten, K. *J. Phys. Chem. B* **2001**, *105*, 10124–10131.
- Birge, R. R.; Gillespie, N. B.; Izaguirre, E. W.; Kusnetzow, A.; Lawrence, A. F.; Singh, D.; Song, W.; Schmidt, E.; Stuart, J.; Seetharaman, S.; et al. *J. Phys. Chem. B* **1999**, *103*, 10746–10766.
- Czege, J.; Rheinisch, L. *Photochem. Photobiol.* **1991**, *53*, 659–666.
- Fischer, T.; Hampp, N. A. *Biophys. J.* **2005**, *89*, 1175–1182.
- Masthay, M. B.; Sammeth, D. M.; Helvenston, M. C.; Buckman, C. B.; Li, W.; Cde-Baca, M. J.; Kofron, J. T. *J. Am. Chem. Soc.* **2002**, *124*, 3418–3430.
- Birge, R. *Acc. Chem. Res.* **1986**, *19*, 138–146.
- Miyawaki, A. *Nat. Rev. Mol. Cell Biol.* **2011**, *12*, 656–668.
- Ellis-Davies, G. C. R. *ACS Chem. Neurosci.* **2011**, *2*, 185–197.
- Albota, M.; Beljonne, D.; Brédas, J.-L.; Ehrlich, J. E.; Fu, J.-Y.; Heikal, A. A.; Hess, S. E.; Kogej, T.; Levin, M. D.; Marder, S. R.; et al. *Science* **1998**, *281*, 1653–1656.
- Cumpston, B. H.; Ananthavel, S. P.; Barlow, S.; Dyer, D. L.; Ehrlich, J. E.; Erskine, L. L.; Heikal, A. A.; Kuebler, S. M.; Lee, I.-Y. S.; McCord-Maughton, D.; et al. *Nature* **1999**, *398*, 51–54.
- Kawata, S.; Kawata, Y. *Chem. Rev.* **2000**, *100*, 1777–1778.
- Yao, B.; Ren, Z.; Menke, N.; Wang, Y.; Zheng, Y.; Lei, M.; Chen, G.; Hampp, N. *Appl. Opt.* **2005**, *44*, 7344–7348.
- Fischer, T.; Neebe, M.; Juchem, T.; Hampp, N. *IEEE Trans. Nanobiosci.* **2003**, *2*, 1–5.
- Peters, J.; Peters, R.; Stoeckenius, W. *FEBS Lett.* **1976**, *61*, 128–134.
- Druckmann, S.; Renthal, R.; Ottolenghi, M.; Stoeckenius, W. *Photochem. Photobiol.* **1984**, *40*, 647–651.
- Oesterhelt, D.; Schuhmann, L.; Gruber, H. *FEBS Lett.* **1974**, *44*, 257–261.
- Möller, C.; Büldt, G.; Dencher, N. A.; Engel, A.; Müller, D. J. J. *Mol. Biol.* **2000**, *301*, 869–879.
- Oesterhelt, D.; Stoeckenius, W. *Methods Enzymol.* **1974**, *31*, 667–678.

- (40) Rhinow, D.; Chizhik, I.; Baumann, R.-P.; Noll, F.; Hampp, N. *J. Phys. Chem. B* **2010**, *114*, 15424–15428.
- (41) Schreckenbach, T.; Walckhoff, B.; Oesterhelt, D. *Eur. J. Biochem.* **1977**, *76*, 499–511.
- (42) Wakatsuki, S.; Kimura, Y.; Stoeckenius, W.; Gillis, N.; Eliezer, D.; Hodgson, K. O.; Doniach, S. *Biochim. Biophys. Acta* **1994**, *1185*, 160–166.
- (43) Brown, L.; Kamikubo, H.; Zimányi, L.; Kataoka, M.; Tokunaga, F.; Verdegem, P.; Lugtenburg, J.; Lanyi, J. K. *Proc. Natl. Acad. Sci. U.S.A.* **1997**, *94*, 5040–5044.
- (44) Rhinow, D.; Hampp, N. *A. J. Phys. Chem. B* **2008**, *112*, 13116–13120.
- (45) Baumann, R.-P.; Schranz, M.; Hampp, N. *Phys. Chem. Chem. Phys.* **2010**, *12*, 4329–4335.
- (46) Cladera, J.; Sábes, M.; Padros, E. *Biochemistry* **1992**, *31*, 12363–12368.
- (47) Wu, S.; El-Sayed, M. A. *Biophys. J.* **1991**, *60*, 190–197.
- (48) Yokoyama, Y.; Negishi, L.; Kitoh, T.; Sonoyama, M.; Asami, Y.; Mitaku, S. *J. Phys. Chem. B* **2010**, *114*, 15706–15711.